The Fifteenth International Symposium on Artificial Life and Robotics 2010 (AROB 15th '10),
B-Con Plaza, Beppu,Oita, Japan, February 4-6, 2010

X-ray Computed Tomography using Material-Class Modeling by Markov Random Field Energy Minimization

Wataru Fukuda, Shin-ichi Maeda, Atsunori Kanemura, and Shin Ishii

Graduate School of Informatics, Kyoto University
Kyoto 611-0011, Japan
fukuda,ichi,atsu-kan,ishii @sys.i.kyoto-u.ac.jp

Abstract: We develop a new statistical reconstruction method for X-ray computed tomography. We utilize the knowledge that the human body is composed of a finite number of material kinds and CT values depend on the material classes. The problem is formulated in the framework of maximum a posterior (MAP) estimation and tomographic image and material classes are simultaneously estimated. To minimize the MAP objective function, we use an expansion algorithm which is a variant of graph cuts.

Keywords: Computed tomography, image reconstruction, metal artifact reduction

I. INTRODUCTION

Computed tomography (CT) is an important medical imaging technology, and a number of CT algorithms for reconstructing tomographic image from a series of X-ray projections have been developed [1–6]. One of the difficulties of CT techniques stems form the requirement for the reducing X-ray exposure in order to avoid overdoes of radiation. However, such limitation on the X-ray exposure would make the observed data noisy or make the amount of the observed data insufficient. Thus, the classical filtered back projection (FBP) and maximum likelihood (ML) solutions become ill-conditioned and unstable. We resolve this ill-poseness by introducing suitable prior knowledge that regularizes the ML solution. As the prior knowledge, we assume that X-ray attenuation coefficients depend on the material classes and the human body is composed of a finite number of material classes; they include soft tissue (fat), normal tissue (muscle), and born.

Another difficulty of CT techniques is metal artifact. It is known that the presence of high density objects such as metal prostheses and dental fillings cause streak or star artifacts when the FBP algorithm is applied [1, 3, 5]. The most popular approach to metal artifact reduction (MAR) is the projection completion method [1]. Although this approach is effective for MAR by detecting and interpolating the metal regions in the sinogram, information from the projections passing through metal may be lost. Even worse, it is not easy to determine the metal regions, especially when two or more metals are inserted. We tackle this MAR problem by a statistical approach, in which we introduce a material class of implanted metal.

Although there are studies that assume the material-class-dependent X-ray attenuation [3–5], most of them estimate the tomographic image and the material classes in a separate manner. Since the estimation of reconstructed image and the material classes are closely related, such separate estimation may deteriorate the reconstruction performance. Therefore, simultaneous estimation for a tomographic image and material classes in term of a consistent cost function is desired. One of such solutions was proposed in [6], which was based on Bayesian inference. Their model consists of the prior probability of the X-ray attenuation coefficients and the likelihood that describes the observation process given X-ray attenuation coefficients. However, due to the high-dimensionality and nonlinear dependency of random variables, they use a simple model and approximation method. In this study, we consider to use a more realistic observation model and a suitable prior distribution. The tomographic image and material classes are estimated by maximum a posteriori (MAP) estimation. Especially, a variant of the graph cut algorithms called an expansion algorithm [7–9] is used for an efficient and accurate MAP estimation.

II. ALGORITHM

Suppose we have T projections $\mathcal{D} = \mathbf{y}^{(1)} \quad \mathbf{y}^{(T)}$ and the tth projection is represented by $\mathbf{y}^{(t)} = y_1^{(t)} \quad y_I^{(t)}$, where $y_i^{(t)}$ denotes the number of photons sensed at detector i when projected from a certain direction $^{(t)}$. Our aim is to reconstruct a tomographic image represented by a J-dimensional vector $\mathbf{x} = x_1 \quad x_J$ obtained by raster scanning the attenuation coefficients.

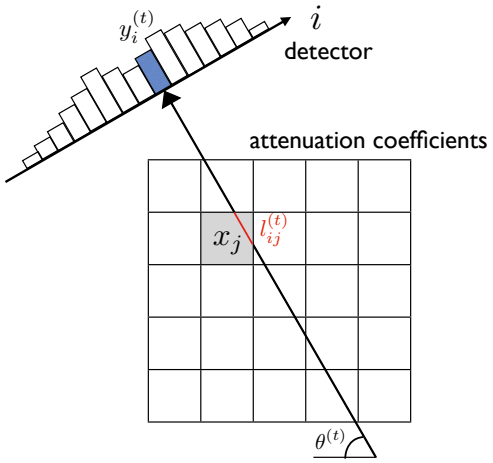

Figure 1: Geometry of CT. x_j is the attenuation coefficient at pixel j, and $l_{ij}^{(t)}$ is the intersection length at pixel j when projected from the direction $^{(t)}$ to the detector i.

1. Observation Model

The data acquisition model is written by

$$\hat{y}_i^{(t)} = b_i^{(t)} \exp \quad \sum_{j=1}^{J} l_{ij}^{(t)} x_j \tag{1}$$

Here, $\hat{y}_i^{(t)}$ denotes the expected number of detected photons, $b_i^{(t)}$ is the number of photons that would be detected in the absence of any absorber, and $l_{ij}^{(t)}$ is the effective intersection length of projection i with pixel j when projected from the direction $^{(t)}$. Fig. 1 illustrates the data acquisition process.

The main source of the fluctuation in the observation is assumed to be arisen from a quantum nature of X-ray photons [2–4]. We represent the fluctuation by an independent Poisson distribution over the measurements:

$$p(\mathcal{D}|\mathbf{x}) = \prod_{t=1}^{T}\prod_{i=1}^{I} p(y_i^{(t)}|\mathbf{x}) = \prod_{t=1}^{T}\prod_{i=1}^{I} \frac{\hat{y}_i^{(t) y_i^{(t)}} e^{\ y_i^{(t)}}}{y_i^{(t)}!} \tag{2}$$

2. Conditional Prior

We incorporate some *a priori* knowledge in reconstruction of tomographic image. We assume that each element of $\mathbf{x}$ is classified into different material classes: air, soft tissue, normal tissue, bone, and implanted metal. We denote the number of classes by K (here, $K = 5$). Thus, the prior $p(\mathbf{x})$ is represented via variables $\mathbf{z} = \ \mathbf{z}_1 \qquad \mathbf{z}_J$:

$$p(\mathbf{x}) = p(\mathbf{x}|\mathbf{z})p(\mathbf{z}) = \prod_{j=1}^{J} p(x_j|\mathbf{z}_j)p(\mathbf{z}_j) \tag{3}$$

Input : Observation $\mathcal{D}$
Output : Estimate of CT value $\hat{\mathbf{x}}$

1 : **until** Convergence criterion is satisfied **do**
2 : Update x_j to minimize (9) by SCG method
3 : Update $\mathbf{z}_j$ to minimize (10) by graph cuts
4 : $\hat{\mathbf{x}}$ $_j$

Figure 2: Proposed algorithm for CT reconstruction.

where $\mathbf{z}_j$ is a K-dimensional binary random vector whose kth element $z_{jk} \in \ 0 \ 1 \ $ is 1 when the pixel j belongs to the kth material class and other elements z_{jk} are 0. Since each pixel belongs to a single material class, $\sum_k z_{jk} = 1$ is satisfied.

When the material class is given, the attenuation coefficients $\mathbf{x}$ are assumed to obey a Gaussian distribution:

$$p(x_j|\mathbf{z}_j) = \prod_{k=1}^{K} \mathcal{N}(x_j| \ _k \ r_k^2)^{z_{jk}} \tag{4}$$

where $_k$ and r_k^2 denote the mean and the variance of the Gaussian distribution, respectively, and r_k^2 was determined irrelevant to the material class (Table 1).

Although the class-wise means $_k$ should be calibrated in advance, this task would not be required for every subject because the values of $_k$ are expected not to vary significantly. Variations of $_k$ due to the unreliability of the CT scanner or the fluctuation of the CT values over different individuals, different organs, or different tissues are assumed to be captured by the randomness of Gaussian distribution, whose uncertainty is controlled by its variance r_k^2.

3. Prior for Class

We give the prior of the material class as the following Boltzmann distribution:

$$p(\mathbf{z}) = \frac{1}{Z} \exp \quad E(\mathbf{z}) \tag{5}$$

where Z is a normalizing constant and the energy is defined by

$$E(\mathbf{z}) = \quad \sum_{k=1}^{K} J_k^{\text{self}} \sum_{j=1}^{J} z_{jk} + J_k^{\text{inter}} \sum_{j=1}^{J} \sum_{s \in \ (j)} z_{jk} z_{sk} \Big) \tag{6}$$

Here, (j) represents the set of pixels adjacent to pixel j, and J^{self} and J^{inter} are nonnegative constants that control the characteristics of the class prior. The Boltzmann distribution takes a high probability when energy $E(\mathbf{z})$ is low. Therefore, the first term of the energy function represents the relative proportion of each material: large J^{self} promotes $z_{jk} = 1$. The second term defines the degree of correlation between neighboring pixels within the material, so as to control the spatial continuity.

Table 1: Parameter settings.

k: material	$_k$	r_k^2 (in §1)	J_k^{self} (in §1)	J^{inter} (in §1)	r_k^2 (in §2)	J_k^{self} (in §2)	J^{inter} (in §2)
1: air	0 000	$10^{\ 6}$	6	30	$10^{\ 6}$	0	50
2: soft tissue	0 018	$10^{\ 6}$	8	30	$10^{\ 6}$	20	50
3: normal tissue	0 022	$10^{\ 6}$	5	30	$10^{\ 6}$	10	50
4: bone	0 050	$10^{\ 6}$	10	30	$10^{\ 6}$	10	50
5: metal	0 120				$10^{\ 6}$	20	50

4. MAP Estimation

According to the Bayes theorem, the posterior distribution for $\mathbf{x}$ and $\mathbf{z}$ is proportional to the product of the prior distribution and likelihood function:

$$p(\mathbf{x}\ \mathbf{z}|\mathcal{D}) \propto p(\mathcal{D}|\mathbf{x})p(\mathbf{x}|\mathbf{z})p(\mathbf{z}) \tag{7}$$

We determine the variable $\mathbf{x}$ and $\mathbf{z}$ by maximizing the posterior probability. Taking the negative logarithm of (7), we can find the solution as a minimizer of the following objective function:

$$L(\mathbf{x}\ \mathbf{z}) = \quad \ln p(\mathcal{D}|\mathbf{x}) \quad \ln p(\mathbf{x}|\mathbf{z}) \quad \ln p(\mathbf{z}) \tag{8}$$

Since the simultaneous optimization for continuous variable $\mathbf{x}$ and discrete variable $\mathbf{z}$ is intractable, we iteratively update each component of the objective function:

$$\mathbf{x}^* = \arg\min_{\mathbf{x}} L(\mathbf{x}\ \mathbf{z}^*) \tag{9}$$

$$\mathbf{z}^* = \arg\min_{\mathbf{z}} L(\mathbf{x}^*\ \mathbf{z}) \tag{10}$$

Here, $\mathbf{x}^*$ is updated using the scaled conjugate gradient algorithm (SCG) and the $\mathbf{z}^*$ is updated by an expansion algorithm, which is a variant of graph cuts [7–9]. The algorithm is terminated when the relative change of $\mathbf{x}$'s norm is smaller than a predetermined threshold $10^{\ 5}$.

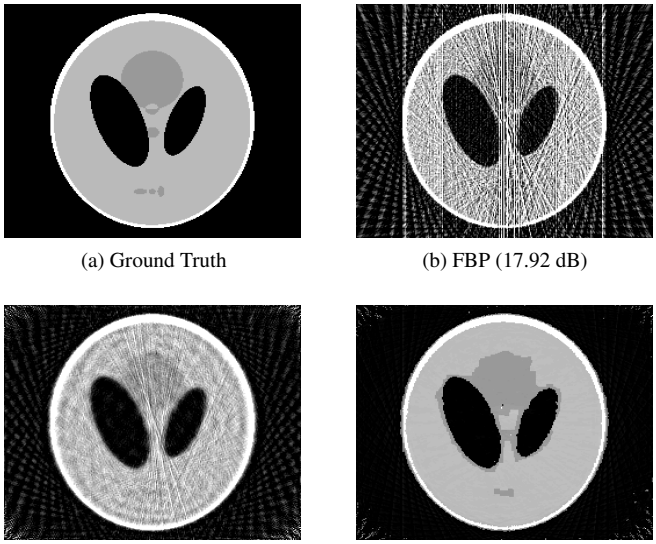

(a) Ground Truth (b) FBP (17.92 dB)

(c) ML (20.96 dB) (d) Proposed (22.58 dB)

Figure 3: Phantom without metal. The window used is [500 500] HU so that the corresponding x_j values are within [0 01, 0 03].

III. EXPERIMENTAL RESULTS

We tested our method by reconstructing phantom images in two severe situations. In the first experiment, the phantom did not include metal, but the number of projections was severely restricted. This setting was prepared to see the reconstruction performance when X-ray exposure was minimized. In the second experiment, metal was inserted into the phantom. This setting was to see how metal artifacts could be reduced by our method.

An attenuation coefficient x can be transformed into the Hounsfield unit (HU) by the following transformation: $1000(x \quad x_0)\ x_0$, where x_0 $(=\ 0\ 02)$ is the attenuation coefficient of water (H_2O).

1. Phantom Data Without Metal

A phantom was created as shown in Fig. 3(a) (471×353 mm ellipse). Parallel beam acquisition was simulated using 367 detectors and 32 projection angles over 180 . The blank scan value b_i was set to 10^5. Images of size 256×256 pixels were reconstructed. The following three different approaches were compared: filtered back projection (FBP), maximum likelihood (ML) [2], and our proposed method. The model parameters were fixed at hand-tuned values: $r_k^2 = 10^{\ 6}$, $J^{\text{inter}} = 30$, $J_1^{\text{self}} = 6$, $J_2^{\text{self}} = 8$, $J_3^{\text{self}} = 5$, $J_4^{\text{self}} = 10$ (Table 1).

The estimation results are shown in Fig. 3. The panels show (a) the ground truth image, reconstructed images by (b) FBP, (c) ML, and (d) the proposed method. The performances were measured by peak signal-to-noise ratio (PSNR), which is shown at the bottom of each panel. The PSNR of our algorithm (22.58 dB) is higher than those by the existing algorithms. The reconstruction results of FBP and ML are very noisy due to the limited number of projections. However, our result is smooth thanks to the prior incorporating the knowledge of material classes knowledge.

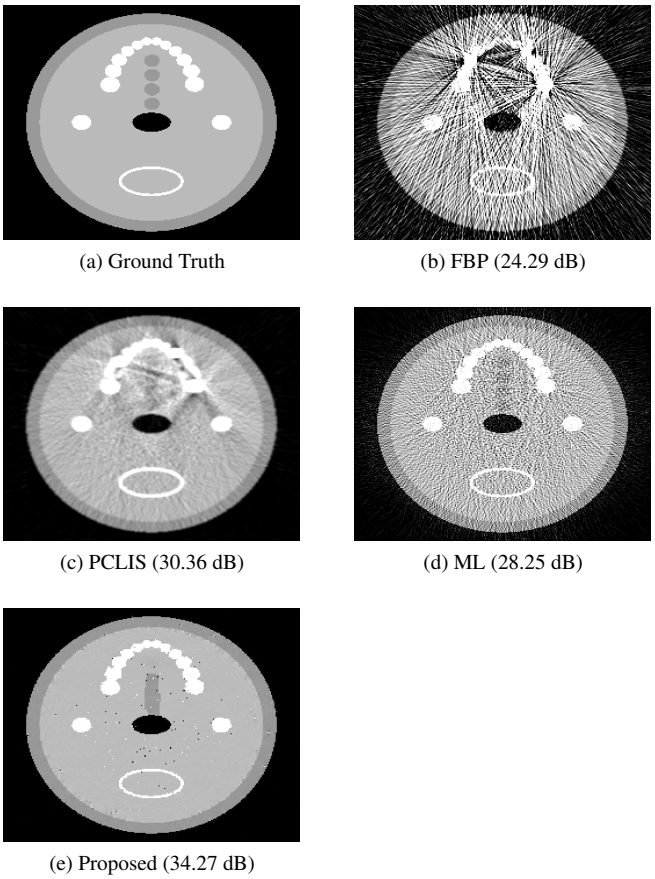

(a) Ground Truth (b) FBP (24.29 dB)

(c) PCLIS (30.36 dB) (d) ML (28.25 dB)

(e) Proposed (34.27 dB)

Figure 4: Phantom without metal. The window used is [500 500] HU so that the corresponding x_j values are within [0 01, 0 03].

2. Phantom Data With Metal Inserted

A head phantom (ellipse 472×436 mm) shown in Fig. 4 was created for the experiment with metal inserted; it includes three dental fillings (three disks with diameters 18, 19, and 23 mm) made of metal. Parallel beam acquisition was simulated using 185 detectors and 1791 projection angles over 180 . The blank scan value b_i was set to 10^5. The size of reconstructed images was 256×256 pixels.

Reconstruction was performed by FBP, ML, the projection completion method based on linear interpolation in the sinogram (PCLIS) [1], and our proposed method. The model parameters were set at hand-tuned values: $r_k^2 = 10^{\ 6}$, $J^{\text{inter}} = 50$, $J_1^{\text{self}} = 0$, $J_2^{\text{self}} = 20$, $J_3^{\text{self}} = 10$, $J_4^{\text{self}} = 10$, $J_5^{\text{self}} = 20$ (Table 1).

The reconstruction results are shown in Fig. 4. The panels show (a) the ground truth, reconstructed images by (b) FBP, (c) PCLIS, (d) ML, and (e) the proposed method. The corresponding PSNR is shown at the bottom of each panel. Our algorithm achieved the highest PSNR (34.27 dB) in the algorithms we compared. Good smoothing within each region was obtained by our method.

IV. CONCLUSION

In this article, we have proposed a new CT reconstruction method based on a statistical approach. The key point of our method was the introduction of the material class which allows the existence of extremely high-dense objects such as metal. Our new method enabled significant reduction of the metal artifacts compared to the existing algorithms. Furthermore, it showed better performance when the metal was not inserted but the signal-to-noise ratio was low due to the limited number of projections. Besides our material class model is beneficial for improving the reconstruction image quality, it would be helpful to detect the tumor and to identify anatomical structures owing to our material class segmentation based on CT values, even in the existence of metal.

REFERENCES

[1] W. A. Kalender, R. Hebel, and J. Ebersberger, "Reduction of CT artifacts caused by metallic implants," in *Radiology*, Aug. 1987, vol. 164, pp. 576–577.

[2] J. Nuyts, B. D. Man, P. Dupont, M. Defrise, P. Suetens, and L. Mortelmans, "Iterative reconstruction for helical CT: a simulation study," *Phys. Med. Bio.*, vol. 43, pp. 729–737, 1998.

[3] C. Lemmens, D. Faul, and J. Nuyts, "Suppression of metal artifacts in CT using a reconstruction procedure that combines MAP and projection completion medical imaging," *IEEE Trans. Med. Imaging*, vol. 28, no. 2, pp. 250–260, Feb. 2009.

[4] I. T. Hsiao, A. Rangarajan, and G. Gindi, "Joint-MAP Bayesian tomographic reconstruction with a gamma-mixture prior," *IEEE Trans. Image Process.*, vol. 11, pp. 1466–1477, 2002.

[5] M. Bal and L. Spies, "Metal artifact reduction in CT using tissue-class modeling and adaptive prefiltering," *Med. Phys.*, vol. 33, no. 8, pp. 2582–2859, 2006.

[6] A. Mohammad-Djafari, "Gauss-Markov-Potts priors for images in computer tomography resulting to jonit optimal reconstruction and segmentation," *Int. J. Tomogr. Stat.*, vol. 11, pp. 76–92, 2008.

[7] Y. Boykov, O. Veksler, and R. Zabih, "Efficient approximate energy minimization via graph cuts," *IEEE Trans. Pattern Anal. Mach. Intell.*, vol. 20, no. 12, pp. 1222–1239, Nov. 2001.

[8] Y. Boykov and V. Kolmogorov, "An experimental comparison of min-cut/max-flow algorithms for energy minimization in vision," *IEEE Trans. Pattern Anal. Mach. Intell.*, vol. 26, no. 9, pp. 1124–1137, Sept. 2004.

[9] V. Kolmogorov and R. Zabih, "What energy functions can be minimized via graph cuts?," *IEEE Trans. Pattern Anal. Mach. Intell.*, vol. 26, no. 2, pp. 147–159, Feb. 2004.